Electronic Supplementary Material (ESI) for Energy & Environmental Science

Supplemental Material for:

Kinetics and Mechanism of Solar-Thermochemical H_2 Production by Oxidation of a Cobalt Ferrite-Zirconia Composite

Jonathan R. Scheffe,[a] Anthony H. McDaniel,[b,*] Mark D. Allendorf,[b] Alan W. Weimer[a]

Model Development:

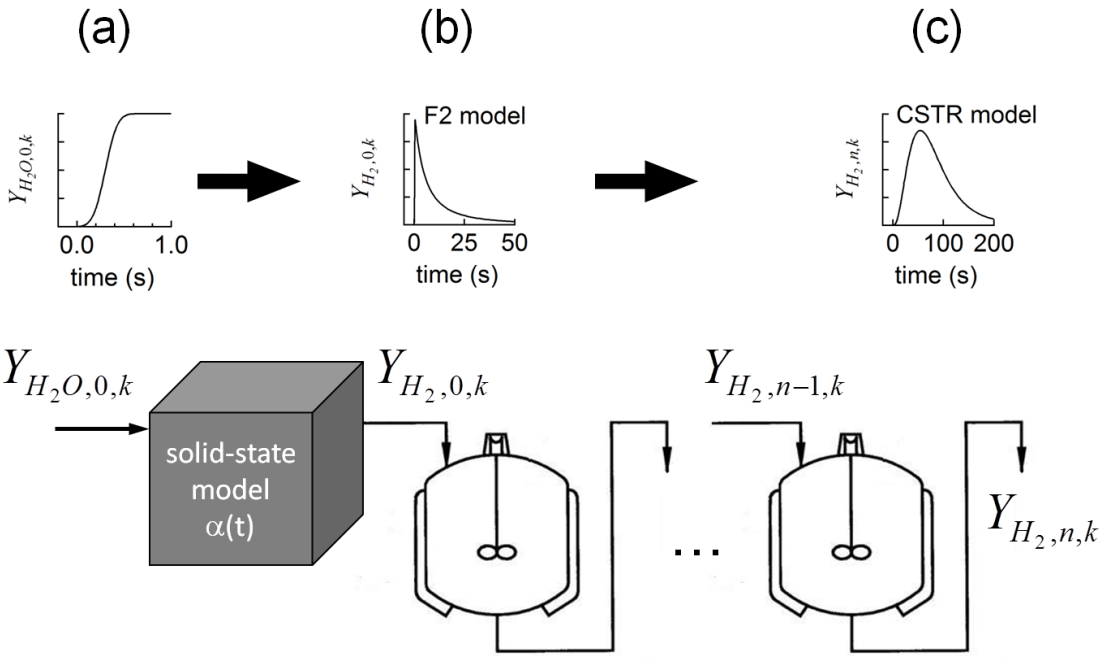

Fig. S1. Schematic representation of the model-based analytical method used to screen kinetic mechanisms and extract rate parameters (see text for discussion).

A numerical approach to analysing the transient H_2 production rates observed during WS was devised that accounts for: 1) kinetic processes occurring in the solid state; 2) the finite time required to introduce water vapour into the reacting volume; 3) detector time lag; and 4) dispersion/mixing of the H_2 evolved from the solid as it is transported downstream of the reactor volume to the detector. Impacts of the aforementioned experimental artefacts (namely 2 – 4 listed above) are not fully addressed by researchers in this field of science even though they can lead to erroneous conclusions regarding both the nature of rate limiting processes and the energetics associated with them.

As shown in figure S1 panel (a), steam is introduced into the reactor volume by way of a step-function input that initiates the solid-state chemistry. We determined the shape of this step-function using a transient, 3-D computational fluid dynamics model of our reactor inlet under various operating conditions (note the minimal dispersion and narrow temporal width of the step). We have also measured similarly rapid gas injection behavior in tracer studies used to determine the space velocity and number of ideal CSTR reactor volumes in the dispersion model (see figure S2). The ensuing chemistry is treated like a black-box that is functionally described by various kinetic models taken from solid-state kinetic theory (panel (b) in figure S1), which track a single variable (α) representing the extent of reaction (i.e., the rate of progress). The output of the black-box is a waveform that describes the temporal evolution of H_2 resulting from the oxidation chemistry and serves as the input molar flow

rate to the first in a series of ideal, continuously-stirred tank reactors (CSTR). The example given here is for model F2, which is a second order relation of the form: $f(\alpha) = (1-\alpha)^2$. Conceptually, the solid-state kinetic model produces a transient pulse-like input of H_2 into the CSTRs that is then stretched in time due to the physical actions of dispersion and mixing (panel (c) in figure S1). Governing kinetic behavior and the associated energetics are deduced by least-squares fitting the experimental H_2 production rate waveforms to simulations based on sampling various solid-state kinetic models.

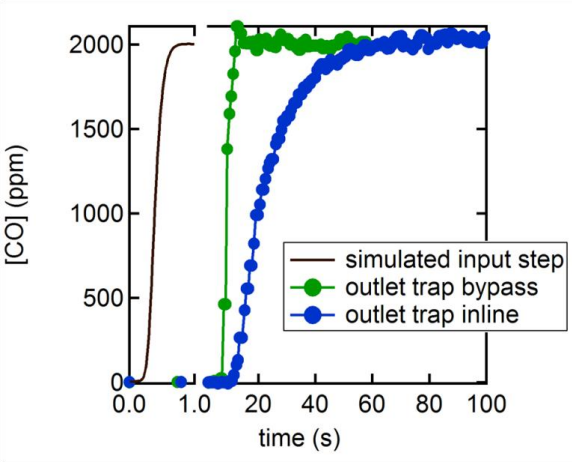

Fig. S2. Concentration of CO as a function of time. The solid line is a simulated input step using an error function, the filled circles are measurements made during a tracer study used to determine the space velocity of well-mixed volume elements in our CSTR model. The green curve is obtained for CO diverted around the cryogenic trap, and the blue curve for CO passing through the cryogenic trap.

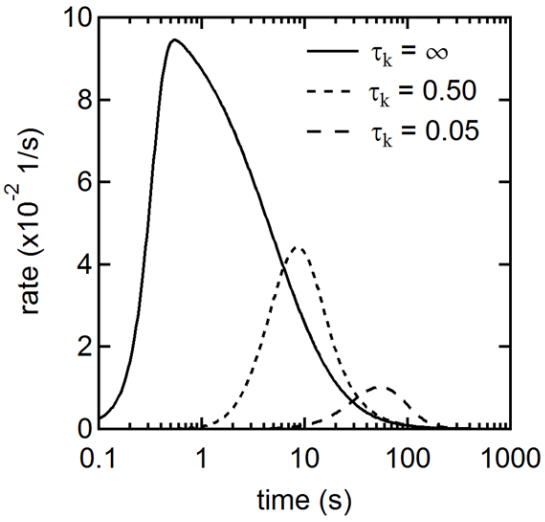

Fig. S3. Simulated production rate curves for the F2 model at a fixed rate constant (k_0 = 0.10 1/s) and three different space velocities (τ_k in 1/s units). An infinite value for the space velocity indicates no dispersion (zero residence time in the CSTR volumes). Decreasing the space velocity increase the CSTR residence time and the dispersion rate.

By comparing the waveforms in panel (b) and (c) of figure S1, it is clear that they have different shapes even though they represent the same kinetic behavior. The extent to which these two curves deviate from one another is dependent on the characteristic time for reaction (kinetic rate, k_0) and the reactor space velocity (dispersion rate, τ_k). Shown in figure S3 are three simulated production rate curves at various space velocities for a dispersion model that includes three CSTR volumes. As

expected, when the space velocity decreases (i.e., greater extent of dispersion) the curves spread out in time and the peak rates decrease in order to conserve total area under each curve. One typical method of analysis reported in this field of research is to take peak rates and cast them into an Arrhenius form such as $\ln k_0 = \ln A_0 - E_0/RT$, then derive the apparent activation energy from the slope of $\ln k_0$ vs. 1/T and the apparent pre-exponential factor from the intercept. If the experimental method is not free of dispersion, then the pre-exponential factor will be erroneous and the reported rates too low.

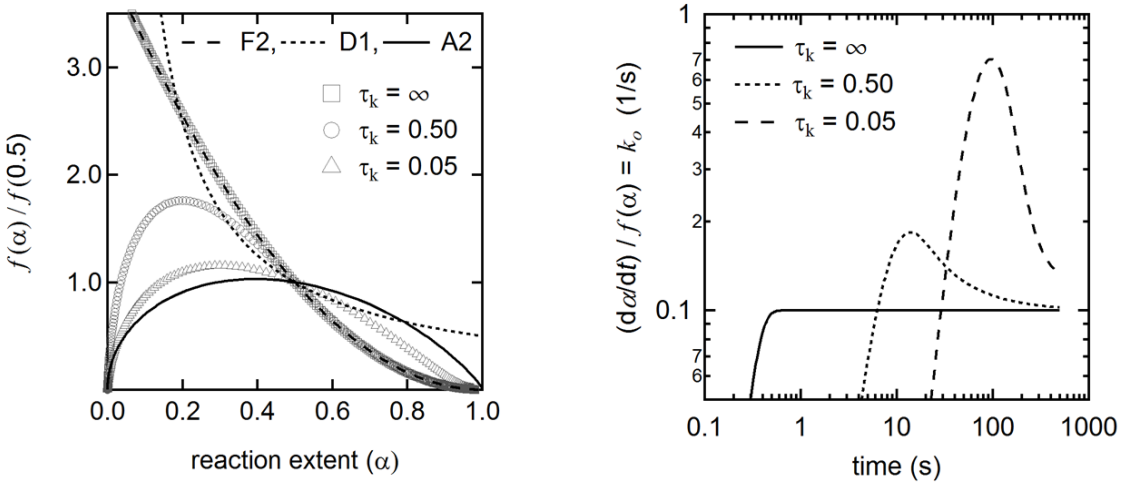

Fig. S4. Simulated Master Plot analysis for the F2 model at a fixed rate constant (k_0 = 0.10 1/s) and three different space velocities (τ_k in 1/s units). An infinite value for the space velocity indicates no dispersion (zero residence time in the CSTR volumes). Decreasing the space velocity increase the CSTR residence time and the dispersion rate. The left panel shows that correct identification of the rate controlling mechanism (F2) only happens at infinite space velocity (the open squares fall on the long-dashed line). Adding dispersion makes the early-time (i.e., low reaction extent) behavior look more like a nucleation model such as A2 could govern this process. The right panel shows how dispersion can lead to an erroneous value extracted for the rate constant assuming the $f(\alpha)$ behavior is known.

We note that the use of solid-state kinetic theory in conjunction with a Master Plot (MP) analysis,[20] without fully addressing how the aforementioned experimental artefacts could influence the analysis, can lead to misinterpretation of the results. We cite the work of {A. Le Gal, S. Abanades, and G. Flamant, Energy & Fuels, 2011, 25, 4836–4845.} in which a MP approach was applied to data obtained in a thermogravimetric analyzer with reactant gases flowing over the sample. In this case, the effects of both the fluid-dynamic environment (dispersion and mixing) in the vicinity of the sample and the residence time of the gas in the system on the analysis are unclear. For example, the statement that the diffusion controlled regime is "delayed" to reaction extents greater than α=0.15 for certain sample preparations is somewhat suspect. In actuality, they are likely attributing the transient initiation of their experimental protocols to an erroneous mechanistic process. Illustrated in the left panel of figure S4 are the results of a Master Plot (MP) analysis conducted on simulated H_2 production rate curves using the F2 model coupled to a dispersion model that includes three CSTR volumes. Here again, as the dispersion rate increases for a fixed reaction rate constant, the shape of the MP curves dramatically change. In fact, the simulated F2 behavior can be completely masked given a sufficiently high rate of dispersion, which would lead to a misidentification of the rate controlling mechanism. In addition, once the rate controlling behavior has been identified (a known $f(\alpha)$), the rate constant can in principle be extracted by plotting $(d\alpha/dt) / f(\alpha)$ vs. time as illustrated in the right panel of figure S4. The correct value for k_0 in this example is 0.10 1/s, which can be seen at infinite space velocity after the initial input transient has abated. The other dashed lines in this figure indicate that the rate constant is variable, implying either an incorrect choice for $f(\alpha)$ or an activation energy that is dependent on the reaction extent.

Mechanism Screening:

Our numerical approach screened 14 individual mechanisms that span four distinct families of solid-state reaction phenomena, including nucleation and growth (A), geometrical contraction or shrinking core (R), diffusion (D), and reaction-order

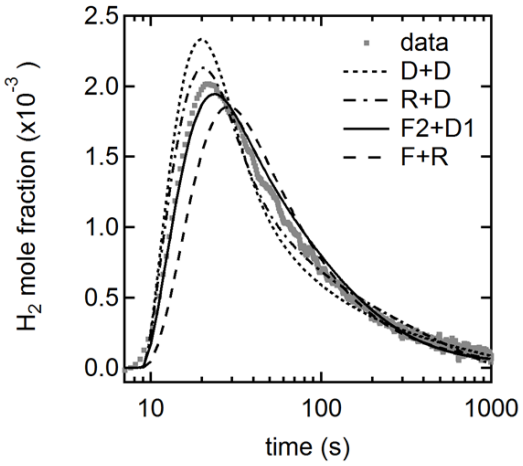

Table ST1. Residual sum of squares (RSSQ) values for various model pairs.

model	RSSQ ($\times 10^{-4}$)
D+D	9.1
R+D	4.6
F2+D1	4.4
F+R	9.2

Fig. S5. H_2 mole fraction as a function of time (solid points) measured at 1100°C and 40 vol.-% H_2O compared to simulations (solid and dashed lines) derived from solid-state kinetic models.

behaviours (F). No single mechanism fit the H_2 production rate across the entire time interval of the experiment. In general, models in the A, R, and F families tend to peak late and *over*-predict H_2 production at longer times, while models in the D family capture the initial peak but consistently *under*-predict H_2 production at longer times. Therefore, two kinetic models were combined to see if a better fit to the experimental observations could be attained. As stated in the main text of this paper, the F2+D1 model pair gives the best fit. The plots in figure S5 and the RSSQ data listed in table ST1 provide further evidence to this statement. Shown in figure S5 are the best fit H_2 mole fractions as a function of time obtained for D+D, R+D, F2+D1, and F+R model pairs compared with the water splitting data for oxidation at 1100°C and 40 vol-% H_2O. Table ST1 lists the associated RSSQ value for each of the model pairs. We believe this analytical approach is sufficiently rigorous to effectively resolve the underlying kinetic behaviour of our ferrite/ZrO_2 composite material, within the context of solid-state kinetic theory, from the confounding affects of the experimental artifacts described in the previous section.

The complete kinetic model is presented in table ST2.

Table ST2. Model rate equations and rate parameters for F2 and D1.

rate expression	A_i 1/s	E_i kJ/mol	γ_i unitless
$\frac{d\alpha_1}{dt} = A_1[Y^0_{H_2O}(t-t_{shift})]^{\gamma_1} \exp[-E_1/RT]\cdot(1-\alpha)^2$	1.92	53.9	1.22
$\frac{d\alpha_2}{dt} = A_2 \exp[-E_2/RT]\cdot\left(\frac{1}{2\alpha}\right)$	85.6	140.7	n/a